Graphical Abstract

Influence of chemisorption on the double hysteresis phenomenon during reactive sputtering

Josja Van Bever, Koen Strijckmans, Diederik Depla

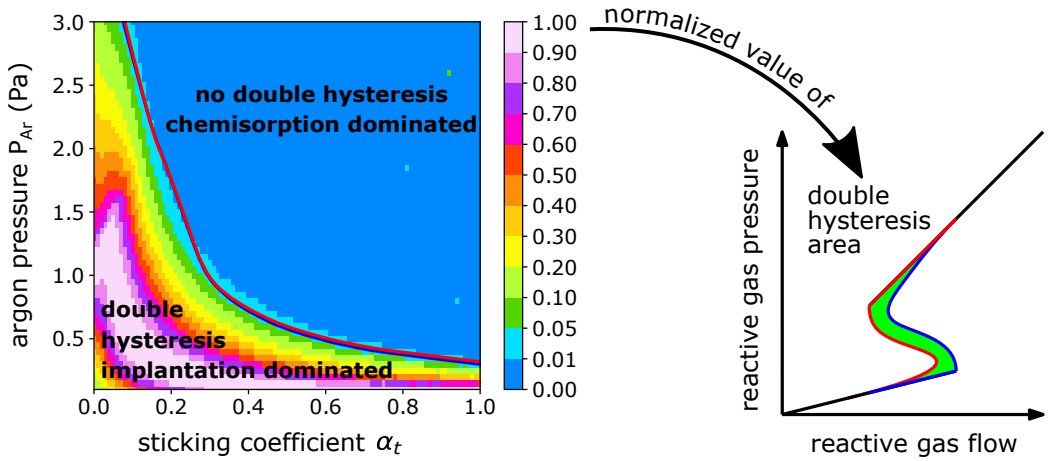

Highlights

Influence of chemisorption on the double hysteresis phenomenon during reactive sputtering

Josja Van Bever, Koen Strijckmans, Diederik Depla

- Quantification of the double hysteresis phenomenon by high throughput modeling
- A description of the impact of reactive gas chemisorption on the double hysteresis
- Derivation of the minimal requirements to observe double hysteresis

Influence of chemisorption on the double hysteresis phenomenon during reactive sputtering

Josja Van Bever[a], Koen Strijckmans[1], Diederik Depla[1]

[a]*Department of Solid State Sciences, Ghent University, Krijgslaan 281, S1, Gent, 9000, , Belgium*

Abstract

Process curves that are obtained during reactive magnetron sputtering can exhibit a double S-shape, also termed a double hysteresis. A previous study mainly focused on the relationship between the double shape behavior and the reaction kinetics of implanted reactive ions, although chemisorption also defines the target condition. As a follow-up study, the influence of chemisorption on double hysteresis is computationally studied by high-throughput calculations using a state-of-the-art model for reactive sputtering. The analysis reveals that the magnitude of the double hysteresis is a conserved quantity for the chemisorption driven reactions at the substrate level. At the target level, a balance between compound formation by direct reactive ion implantation and chemisorption is established. A minimal condition for double hysteresis is derived and process conditions are identified for which the double hysteresis can be measured for target materials prone to strong chemisorption of the reactive gas. The condition can assist to further explore the close interplay between chemisorption and implantation during reactive sputtering.

Keywords: reactive sputtering, target poisoning, modeling

1. Introduction

During reactive magnetron sputtering, target poisoning occurs due to the interaction of the reactive gas, for example oxygen, with the metallic target. Target poisoning has been studied by modeling for several years, because a fundamental understanding is a necessity to optimize the control of the reactive process [1, 2, 3, 4]. Initially, target poisoning was attributed to chemisorption, which is the formation of a compound monolayer due to

the chemical interaction of the target surface with the neutral reactive gas atoms [1]. Both experiments and simulations showed the importance of at least three additional processes [5, 6, 7, 8, 9]. First, chemisorbed material can be knocked into the target subsurface by ions of the working gas (often argon). This is known as knock-on implantation. Secondly, reactive gas ions can be formed inside the gas discharge and are implanted directly into the target. This is termed direct implantation. Finally, redeposition of sputtered atoms can also contribute to target poisoning but is mainly important at high pressures, low mass of the target atoms and/or for specific set-ups such as facing target sputtering [9] and rotating cylindrical magnetrons [7, 8]. A schematic overview of the aforementioned processes is shown in Figure 1.

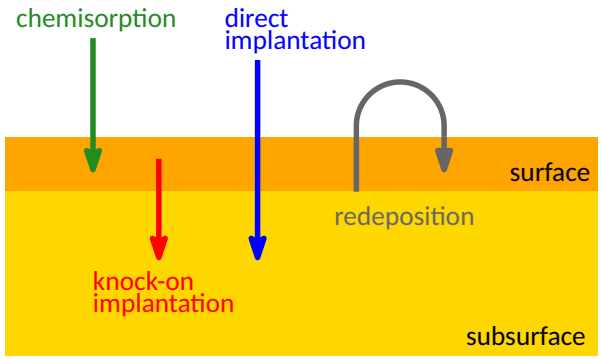

Figure 1: Schematic overview of processes that can induce target poisoning.

When the reactive gas flow is stepwise increased during reactive sputtering, target poisoning often occurs abruptly at a single reactive gas flow. The transition back from the poisoned target state to the metal target state also happens abruptly in these cases, but at a lower reactive gas flow. This is known as hysteresis. The abrupt changes can be seen in deposition parameters, for example the reactive gas pressure, the deposition rate and the discharge voltage. The hysteresis behavior was successfully explained by Berg *et al.*. [1] using a single S-shaped process curve of each deposition parameter as a function of the reactive gas flow. Hence, this hysteresis will be termed a "single" hysteresis, to distinguish it from the double hysteresis discussed further.

When feedback control is used [10], the abrupt transition can be circumvented. During feedback control, a stepwise change of one or a combination of more deposition parameters is achieved by continuously controlling the

reactive gas flow to fix the target condition. This way, the metal to poison transition of the target as well as the reverse transition can be studied in a continuous way. This results in S-shaped process curves, but the curve corresponding to the transition from a metallic target to a poisoned target often does not coincide with the curve corresponding to the reverse transition [10, 11, 12, 13]. This double S-shape has been termed double hysteresis [13]. The S-curve connected to the transition from a metallic to a poisoned target is defined as the metal branch while the poison branch refers to the second S-curve. It should be noted that the two S-curves can be distinguished, even when effects due to e.g. chamber heating or target erosion are excluded [13].

In our previous paper [14] the double hysteresis was computationally studied, and its origin was quantitatively explained. The implanted reactive gas ions have a limited time to react with the target material before they are removed by sputtering. For the poison branch, the erosion speed is low, and hence there is sufficient time to react, but the opposite is valid for the metal branch. It was demonstrated that the double hysteresis behavior originates from this difference in removal rate.

The aforementioned mechanism was elucidated based on high throughput simulations using a data set obtained from a detailed study of the Al/O_2 system [4]. Quite specific for this material/reactive gas combination is the low value (0.1) of the target sticking coefficient of oxygen on aluminum. Hence, the influence of chemisorption on the obtained results can be expected to be small. However, for more reactive metals, chemisorption onto the target surface will contribute stronger to target poisoning. In this paper the influence of chemisorption, both at target and substrate level, on the double hysteresis behavior is studied.

The article is structured as follows. In Section 2, we briefly discuss the model and analysis techniques used and introduce the main concepts for the relations derived later on. The influence of chemisorption on the double hysteresis is the main subject of Section 3. Chemisorption affects both the substrate (Section 3.1) and the target (Section 3.2). It is shown that only chemisorption at the target level affects the double hysteresis behavior. A minimal condition (Section 3.3) for double hysteresis is derived and used to maximize the double hysteresis behavior for target materials with a high sticking coefficient. A summarizing discussion is presented at the end of the paper, where also suggestions are made on how these findings can be applied in experiments.

2. Modeling and analysis techniques

2.1. RSD-model

The RSD-model [2, 15, 4] describes the reactive sputtering process by a coupled set of partial differential equations. These differential equations govern the time evolution of the properties of the vacuum chamber, the substrate and the target. The model focuses on the quantitative description of target processes. It is to the best knowledge of the authors the only model that is able to describe double hysteresis during reactive sputtering. The model is implemented in a freely available software package [16]. Details on the model can be found in the references [2, 15, 4, 14]. To ensure a good readability, the same symbols as in Van Bever *et al.* [14] have been used in this paper.

In the remainder of the paper, only equations required for an understanding of the obtained results are given in order to guide the discussion. It must be noted that the substrate and target are spatially resolved within the model by the deposition profile and the ion current density respectively. In order to simplify the notation, the equations used further in the text are written for a single cell approximation. For example, the ion current density should be denoted by $j_{ion,m}$ for every target cell m separately. In the following, the notation j_{ion} is however used. The derivations are nonetheless equally valid for a multi-cell approximation.

2.2. Quantification of hysteresis

For our analysis, abstraction is made of the exact shape of the process curves. Instead, hysteresis quantification measures were introduced [14]. These are measures that can be linked to changes of the hysteresis curve and demonstrate continuous trends as a function of process and material parameters.

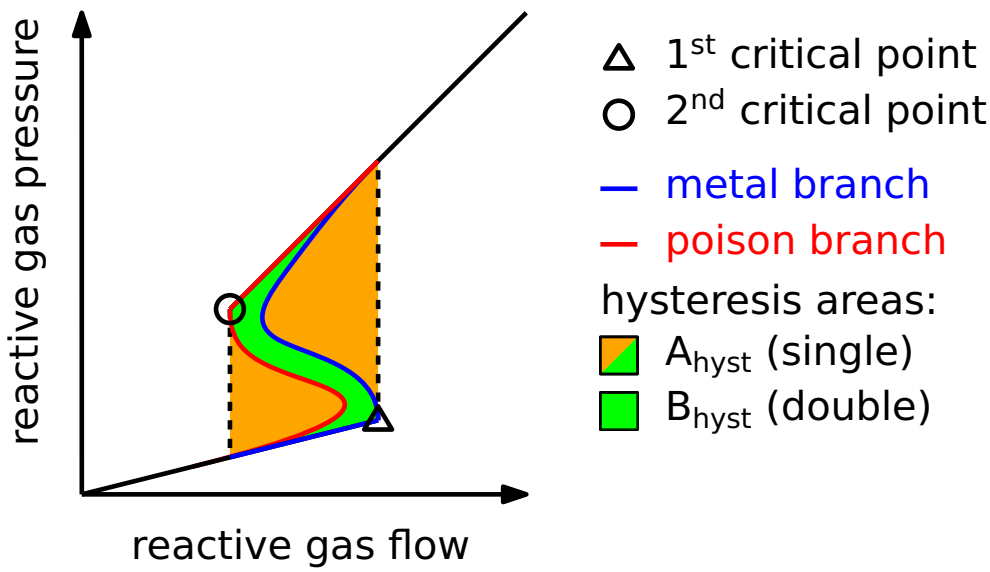

Figure 2: Depiction of the main hysteresis quantification measures when measuring the reactive gas pressure as a function of the reactive gas flow. The critical points and A_{hyst} are used to analyze hysteresis under flow control. The branches and B_{hyst} are used to study hysteresis under feedback control.

The main hysteresis quantification measures are indicated in Figure 2 on a reactive gas pressure P_{R_2} versus reactive gas flow Q_{R_2} process curve. To quantify the magnitude of a double hysteresis, the double hysteresis area B_{hyst} is used. This area depends on the type of process curve considered, which is indicated within square brackets e.g. B_{hyst} $[P_{\text{R}_2}(Q_{\text{R}_2})]$. To analyze the double hysteresis behavior, the branch averaged values are used. These are obtained from the transition paths between the metallic and poisoned mode indicated in Figure 2 (blue and red). The branch averaged value of a property X over the metal or poison branch is denoted by $\overline{X}$ $[m]$ or $\overline{X}$ $[p]$ respectively.

In a similar way as for double hysteresis, the single hysteresis area A_{hyst} and critical points are used to understand hysteresis under flow control. These are also indicated in Figure 2.

The calculation of hysteresis quantification measures and further analysis techniques are implemented in `RSDplot`. [17]

2.3. High-throughput analysis

The high-throughput analysis of Van Bever *et al.* [14] was continued. The process and material parameters in the RSD-model are first scanned over a wide range. The information of this large data set is then studied based on the hysteresis quantification measures (Section 2.2) to understand the impact of a given parameter on the evolution of the double hysteresis behavior. Here, we focus on parameters that are related to chemisorption. The compound formation at the substrate level is described by chemisorption and deposition. The corresponding reactive gas consumption rate is defined by the substrate area A_s and the sticking coefficient α_s. The "substrate" is defined as the total surface on which deposition occurs, including the walls of the vacuum chamber itself. A competing process for reactive gas consumption is the action of the physical pump with a pumping speed equal to S. At the target level, the main parameter that defines the chemisorption is the target sticking coefficient α_t. Finally, it will follow from the minimal condition (Section 3.3) that also the argon pressure P_{Ar} should be considered. Other process and material parameters, which can have an indirect influence on chemisorption as well, were used to verify the proposed mechanisms. In our analysis we try to be as general as possible. It should however be stressed that the original data set was obtained based on the aluminum reference system discussed in our previous work [4].

The considered hysteresis measures (Section 2.2) were converged with respect to the number of simulated steady-state pressure points ($\geqslant 1000$) and the number of target cells ($\geqslant 300$).

3. Results: influence of chemisorption on double hysteresis

3.1. Substrate and chamber

As an example of the impact of the substrate and the chamber conditions on the double hysteresis, the influence of the substrate area and the pumping speed is treated.

First, a reference system was considered that exhibits a clear double hysteresis (identified as reference A (see Appendix A) and represented with squares in Figure 3). The double hysteresis area B_{hyst} (see Section 2.2) remains constant if the pumping speed is modified, although the process curves and the single hysteresis area do change (not shown). The change of the single hysteresis can be related to the balance between the reactive gas flow to the pump Q_p and the reactive gas consumption rate by the substrate Q_s in

a similar fashion as originally modeled by Berg and Nyberg [1]. The same is also true for the substrate area, except at very small substrate areas, for which a decrease of the double hysteresis area is observed.

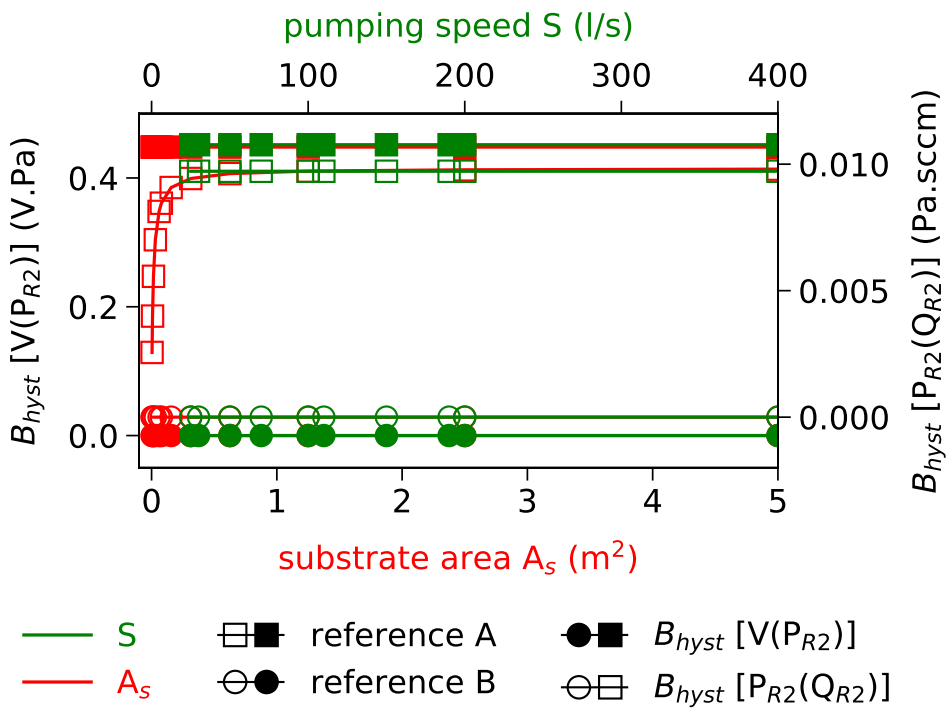

Figure 3: Influence of the substrate area (bottom axis) and pumping speed (upper axis) on the double hysteresis. The data was generated by a change of the considered parameter only. A reference was used that either exhibits a double hysteresis (squares, see Appendix A) or no double hysteresis (circles, obtained from Appendix A by changing the target area A_t to 80 cm^2 and the reaction rate constant k to $5 \cdot 10^{-23}$ cm^3/s). The double hysteresis area was obtained for either the discharge voltage versus reactive gas pressure diagram ($B_\mathrm{hyst}[V(P_\mathrm{R_2})]$, filled symbols, left axis) or the reactive gas pressure versus flow diagram (B_hyst $[P_\mathrm{R_2}(Q_\mathrm{R_2})]$, empty symbols, right axis).

To investigate the deviation at small substrate areas, the double hysteresis area was calculated for two sets of process curves. $B_\mathrm{hyst}[P_\mathrm{R_2}(Q_\mathrm{R_2})]$ is calculated from the reactive gas pressure $P_\mathrm{R_2}$ versus flow $Q_\mathrm{R_2}$ process curve, while $B_\mathrm{hyst}[V(P_\mathrm{R_2})]$ originates from the process curve when the discharge voltage V is plotted against the reactive gas pressure $P_\mathrm{R_2}$. A breakdown at very small substrate areas is observed for $B_\mathrm{hyst}[P_\mathrm{R_2}(Q_\mathrm{R_2})]$ but not for $B_\mathrm{hyst}[V(P_\mathrm{R_2})]$.

This can be explained as follows. The reactive gas pressure that corresponds in steady-state to a certain reactive gas flow is determined by the reactive gas consumption inside the vacuum chamber, which is modeled as follows:

$$\frac{dP_{\mathrm{R}_2}}{dt} = \frac{k_{\mathrm{B}}T}{\mathcal{V}}\frac{dN_{\mathrm{R}_2}}{dt} = \frac{k_{\mathrm{B}}T}{\mathcal{V}}\left(Q_{\mathrm{R}_2} - Q_{\mathrm{p}} - Q_{\mathrm{s}} - Q_{\mathrm{t}}\right), \tag{1}$$

with k_{B} the Boltzmann constant, T and $\mathcal{V}$ the temperature and the volume of the vacuum chamber, and N_{R_2} the number of R_2 gas molecules inside the vacuum chamber. The evolution of N_{R_2} depends on the reactive gas flow Q_{R_2} entering the chamber and the R_2 flows consumed by the pump (Q_{p}), substrate (Q_{s}), and target (Q_{t}).

The largest contribution to this consumption is either the reactive gas flow going to the substrate or to the pump when operating in metallic or poisoned mode respectively. As the flow towards the target is small, it follows from Equation (1) that when there is no substrate present, the steady-state pressure is only defined by the action of the pump. This leads in the model to

$$P_{\mathrm{R}_2} = k_{\mathrm{B}}T \cdot \frac{Q_{\mathrm{p}}}{S} \approx k_{\mathrm{B}}T \cdot \frac{Q_{\mathrm{R}_2}}{S} \tag{2}$$

This is a linear relation that cannot exhibit any hysteresis. Therefore, for a disappearing substrate, $B_{\mathrm{hyst}}[P_{\mathrm{R}_2}(Q_{\mathrm{R}_2})]$ must become zero. Stated in another way, the reactive gas consumption by reaction of the material deposited onto the substrate is required to observe any hysteresis in the $P_{\mathrm{R}_2}(Q_{\mathrm{R}_2})$ process curve. From a practical point of view, it should be remarked that the breakdown of $B_{\mathrm{hyst}}[P_{\mathrm{R}_2}(Q_{\mathrm{R}_2})]$ occurs for substrate areas that are smaller than for almost any realistic vacuum chamber.

Within the approximations of the RSD-model, the target state is determined by the reactive gas fraction [15] and the discharge voltage can be determined from the target state by using the IV-characteristics of the magnetron sputtering discharge [15, 14]. Hence, the lack of a substrate does not affect the $V(P_{\mathrm{R}_2})$ process curve and $B_{\mathrm{hyst}}[V(P_{\mathrm{R}_2})]$ does not disappear.

Stated more intuitively, the value of $B_{\mathrm{hyst}}[V(P_{\mathrm{R}_2})]$ is directly related to the target state while the value $B_{\mathrm{hyst}}[P_{\mathrm{R}_2}(Q_{\mathrm{R}_2})]$ requires the connection between the target state and the chamber condition via the sputter deposition onto the substrate. This is in agreement with our earlier discussion [14], where it was remarked that a direct interpretation of $B_{\mathrm{hyst}}[P_{\mathrm{R}_2}(Q_{\mathrm{R}_2})]$ is complicated by for example the discharge voltage dependency of the sputter yields. In what follows, we will therefore focus the analysis on $B_{\mathrm{hyst}}[V(P_{\mathrm{R}_2})]$.

The observed trends suggest that double hysteresis is independent of the substrate area and the pumping speed. To verify this hypothesis, a new reference was used (called reference B and represented with circles in Figure 3). This new reference does not exhibit a double hysteresis. When the substrate area or pumping speed of the new reference system is changed, the double hysteresis area remains zero regardless the considered process curve. This confirms the idea that the double hysteresis effect is in general independent of the substrate area and the pumping speed. This trends is also confirmed when the reference system is changed in different ways.

The influence of other substrate and chamber related parameters is similar. For example, the influence of the substrate sticking coefficient α_{s} can be mapped onto that of the substrate area. Other parameters act on both the substrate or chamber condition as well as on the target processes. E.g. an increase of the gas temperature slightly lowers the amount of target chemisorption since the flux F_{R_2} towards the target is lowered. Indeed, from kinetic gas theory it follows that

$$F_{\mathrm{R}_2} = \frac{P_{\mathrm{R}_2}}{\sqrt{2\pi m_{\mathrm{R}_2} k_{\mathrm{B}} T}}, \tag{3}$$

where m_{R_2} denotes the mass of a gas molecule R_2. The decrease in chemisorption influences the balance between chemisorption and implantation (see Section 3.2) and induces a small increase of the double hysteresis area.

3.2. Balance between implantation and chemisorption

Calculations were performed using the reference system from Appendix A. The target sticking coefficient α_{t} was varied. The target sticking coefficient defines the reactive gas consumed at the target level by chemisorption,

$$Q_{\mathrm{t,chem}} = \alpha_t F_{\mathrm{R}_2} \theta_{\mathrm{m}} A_{\mathrm{t}}, \tag{4}$$

where A_{t} is the target area, θ_{m} the metal fraction of the target surface, and F_{R_2} the flux towards the target as defined in equation (3). The trends of the branch averaged values were analyzed. Fig. 4 shows the result. As the sticking coefficient increases, the double hysteresis vanishes (black trace).

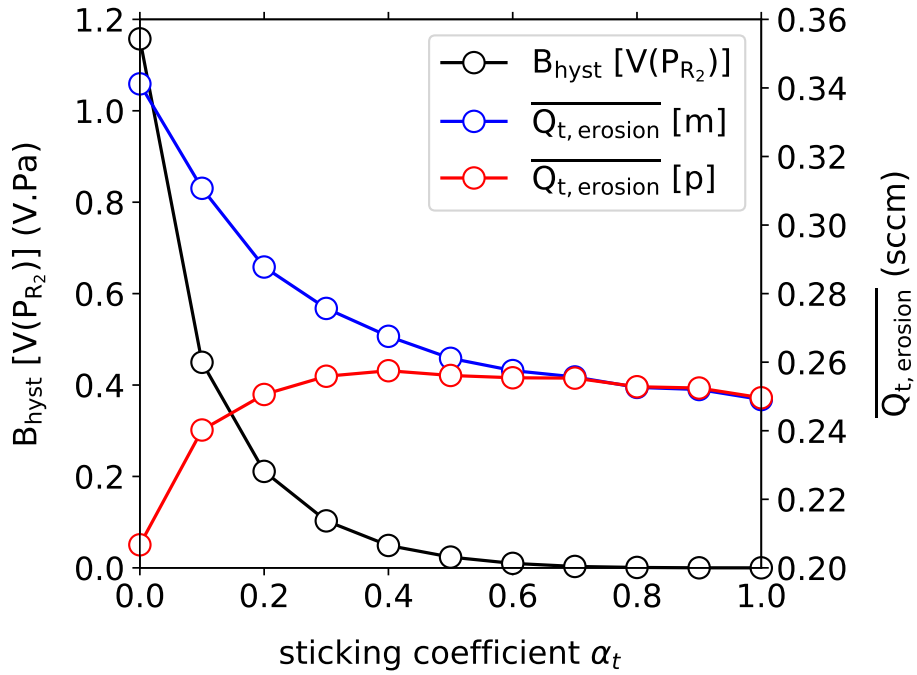

Figure 4: Influence of the target sticking coefficient α_{t} on the double hysteresis behavior. The other simulation parameters were kept constant (see Appendix A). Left axis: the double hysteresis area in the $V(P_{\mathrm{R}_2})$ process curve ($B_{\mathrm{hyst}}[V(P_{\mathrm{R}_2})]$, black). Right axis: the removal rate of non-reacted species for the metal branch (m) and poison branch (p).

As mentioned before, the double hysteresis behavior is defined by the difference in removal rate of the non-reacted ions by sputtering in the metal and poison branch. This removal rate is given by,

$$Q_{\mathrm{t,erosion}} = \frac{1}{2} v_{\mathrm{s}} n_{\mathrm{R}}(0)\, A_{\mathrm{t}} \tag{5}$$

with v_{s} the speed at which the target surface recedes due to erosion and $n_{\mathrm{R}}\,(0)$ the concentration of non-reacted ions at the target surface. The simulations show that the average metal branch removal rate $\overline{Q_{\mathrm{t,erosion}}}\,[m]$ decreases with an increasing sticking coefficient while the opposite occurs for the average poison branch removal rate $\overline{Q_{\mathrm{t,erosion}}}\,[p]$. This behavior can be understood as follows. Within the metal branch, non-reacted species are efficiently removed by the high erosion rate. The reduction of the metal fraction θ_{m} by

an enhanced chemisorption suppresses this effect because the sputter yield of the compound is lower as compared to the metal. Within the poison branch the compound removal is slow as the erosion rate is low. Due to the enhanced chemisorption, target poisoning occurs at lower reactive pressures and hence less reactive species are implanted. This results in a lower compound fraction θ_r of the target which enhances the erosion rate and hence $\overline{Q_{\mathrm{t,erosion}}}\,[p]$. Therefore, the two branch averaged values of $Q_{\mathrm{t,erosion}}$ converge and the double hysteresis disappears.

A more intuitive way to understand this is the following. Chemisorption can efficiently poison the target without requiring implanted ions to be involved. Consequently, when the effect of chemisorption starts to dominate over direct implantation, the metal branch becomes more poisoned (the metal fraction θ_{m} decreases), while the poison branch becomes more metallic (the compound fraction θ_{r} decreases). As a result, the target state becomes equal for both branches and the double hysteresis vanishes.

The result demonstrates that chemisorption can effectively influence the magnitude of the double hysteresis observed. For combinations of target material and reactive gas that exhibit a high sticking coefficient, the double hysteresis can even disappear completely. It is therefore interesting to study the point at which the effect of chemisorption starts to dominate over direct implantation.

3.3. Minimal condition for double hysteresis

The difference in removal rate $Q_{\mathrm{t,erosion}}$ is a good but general tool to define whether or not double hysteresis will be observed. It is however not specific enough to elucidate the impact of chemisorption. As target poisoning is induced in the RSD-model by chemisorption and ion implantation, it is possible to calculate a rate for each compound formation mechanism i.e. P_{chem} and P_{impl}. Their relative weights allow for the determination of the dominating poisoning mechanism.

The formation rates by chemisorption and direct implantation are considered in more detail below. The discussion is schematically depicted in Figure 5.

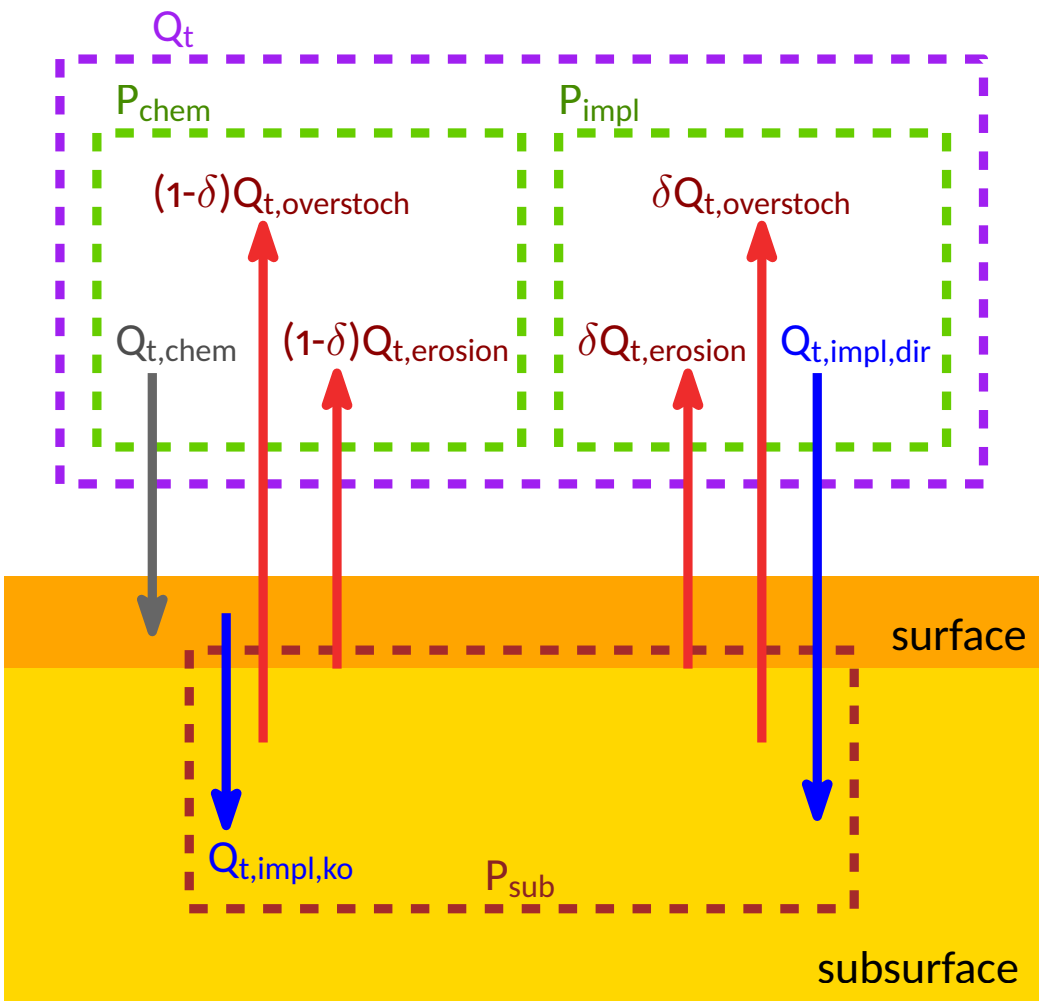

Figure 5: Overview of the flows towards the target and the defined consumption rates. The total reactive gas flow consumed by the target Q_{t} is the result of the reaction of the target material at the target surface by chemisorption ($Q_{\mathrm{t,chem}}$) and in the subsurface region by implanted ions (P_{sub}). The implanted ions originate from two channels: direct implantation ($Q_{\mathrm{t,impl,dir}}$) and knock-on implantation ($Q_{\mathrm{t,impl,ko}}$). Implanted ions that do not react are released from the target (red arrows) by sputter removal ($Q_{\mathrm{t,erosion}}$) or diffuse directly from the target when the subsurface is overstoichiometric ($Q_{\mathrm{t,overstoch}}$).

First of all, the sum of the two formation rates yields the total compound formation at the target. In steady-state, this equals the reactive gas flow

towards the target, Q_{t},

$$Q_{\mathrm{t}} = P_{\mathrm{impl}} + P_{\mathrm{chem}}. \tag{6}$$

Indeed, in steady-state, the amount of non-reacted reactive ions inside the target remains constant. The target flow can therefore be formally attributed to compound formation that is required to compensate for the sputter removal.

The calculation of the formation rates by chemisorption and direct implantation is complicated by additional processes that define the target condition. First, not all implanted atoms are converted to compound as some will reach the target surface without reaction. These atoms are either removed from the target by target erosion or they are assumed to diffuse from the target when the saturation limit for non-reacted atoms is reached. The saturation limit is reached when the formed compound becomes overstoichiometric. Secondly, knock-on implantation converts chemisorbed atoms into implanted atoms that may also subsequently escape from the target. The calculation can nevertheless be performed as discussed in the following paragraphs.

The compound formation rate due to implanted ions in the subsurface region, P_{sub}, is considered first. This formation rate is assumed to result from a second order reaction between the non-reacted implanted ions (concentration n_{R}) and the pure target metal (concentration n_{M}), both at a corresponding depth x and time t. Integration over the total target volume, excluding the target surface, yields

$$P_{\mathrm{sub}} = \frac{1}{2} \int zk \cdot n_{\mathrm{R}}(x,t)\, n_{\mathrm{M}}(x,t)\, dx. \tag{7}$$

Herein, k denotes the reaction rate constant and z the stoichiometry of the formed compound. In order to simplify the further discussion, the rate is expressed in terms of R_2 per time unit rather than MR_{z} per time unit, which explains the factor 1/2.

Within the approximations of the RSD-model, two other processes govern the time evolution of the concentration of non-reacted implanted ions n_{R}, namely the gain due to implantation, direct or knock-on, and losses due to sputter erosion or due to out-diffusion when the formed compound is overstoichiometric. As a consequence, it follows from Equation (7) that in

steady-state ($\partial n_R/\partial t = 0$)

$$P_{\text{sub}} = (Q_{\text{t,impl,dir}} + Q_{\text{t,impl,ko}}) - (Q_{\text{t,erosion}} + Q_{\text{t,overstoch}}) \,. \tag{8}$$

The first two terms describe the target flows due to direct implantation and knock-on implantation. The last two terms account for non-reacted implanted atoms that leave the target by target erosion or are assumed to diffuse from the target when the saturation limit is reached. All terms have been described in our previous paper[14] except for $Q_{\text{t,impl,ko}}$. The flow due to knock-on implantation is defined as

$$Q_{\text{t,impl,ko}} = j_{\text{ion}} \, \frac{1}{2} \beta_{\text{c}} \theta_{\text{c}}. \tag{9}$$

where j_{ion} is the ion current density, θ_{c} the fraction of the target covered with compound formed by chemisorption, and β_c a knock-on yield. In order to compare it with other target flows, it is defined as an amount of R_2 molecules per time, though no physical diatomic gas molecules are implanted.

As seen from Equation (8), the implantation of reactive ions has two sources i.e. direct and knock-on implantation. The loss of non-reacted implanted ions is however independent of the implantation mechanism. Consider therefore the directly implanted part P_{impl} of the compound formation rate by re-scaling P_{sub} with a fraction

$$\delta = \frac{Q_{\text{t,impl,dir}}}{Q_{\text{t,impl,dir}} + Q_{\text{t,impl,ko}}}, \tag{10}$$

This permits the compound formation rate to be calculated as

$$P_{\text{impl}} = Q_{\text{t,impl,dir}} - \delta \, (Q_{\text{t,erosion}} + Q_{\text{t,overstoch}}) \tag{11}$$

The chemisorption part P_{chem} of the compound formation rate is obtained by considering the complementary part of the total compound formation. In steady-state, this can be obtained from Equation (6) as $Q_{\text{t}} - P_{\text{impl}}$, or

$$P_{\text{chem}} = Q_{\text{t,chem}} - (1 - \delta) \, (Q_{\text{t,erosion}} + Q_{\text{t,overstoch}}) \tag{12}$$

At this point, the compound formation rates by chemisorption and ion implantation are obtained, and Fig. 6 presents the calculated values for P_{chem}

and P_{impl} averaged over the two branches. For the dark grey region the condition $P_{\mathrm{chem}} > P_{\mathrm{impl}}$ holds. It is clear that the requirement $P_{\mathrm{impl}} > P_{\mathrm{chem}}$ is a necessity to observe double hysteresis.

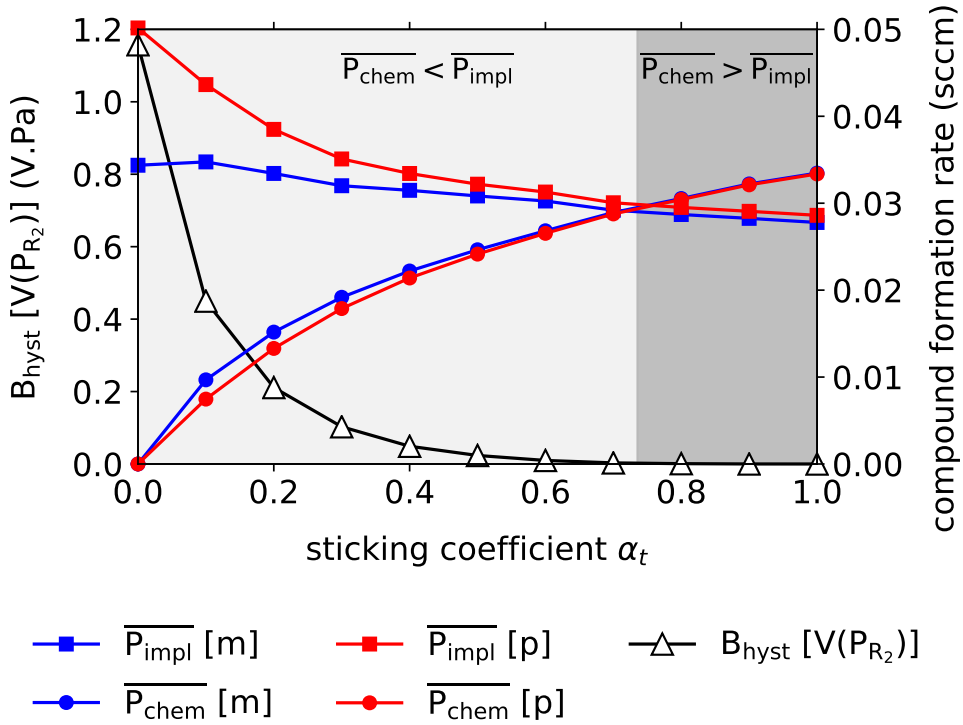

Figure 6: Influence of the target sticking coefficient α_{t} on the double hysteresis behavior. The other simulation parameters were kept constant (see Appendix A). Left axis: the double hysteresis area in the $V(P_{\mathrm{R}_2})$ process curve ($B_{\mathrm{hyst}}[V(P_{\mathrm{R}_2})]$, black). Right axis: the compound formation rates due to direct implantation P_{impl} and chemisorption P_{chem}, averaged over the metal (blue) or poison (red) branch (Equation (12) and Equation (11)). When the compound formation rate P_{chem} becomes larger than the compound formation rate by direct ion implantation P_{impl}, the double hysteresis effect vanishes.

To verify the validity of this minimal condition, another broader set of simulations was performed where both the target sticking coefficient α_{t} and the argon pressure P_{Ar} are varied.

From Figure 7 it is observed that the double hysteresis area B_{hyst} obtained from the $V(P_{\mathrm{R}_2})$ process curve decays to zero for large argon pressures. This trend is compared to the branch averaged values of the compound formation

rates by direct implantation (P_{impl}) and chemisorption (P_{chem}). The argon pressure at which the compound formation rates by chemisorption and direct implantation become equal, corresponds with the value at which the double hysteresis behavior is not observed anymore. This is only approximately true since averaged values are considered. At the transition pressure indicated in Figure 7, some target cells and/or samples inside each branch are still dominated by direct implantation.

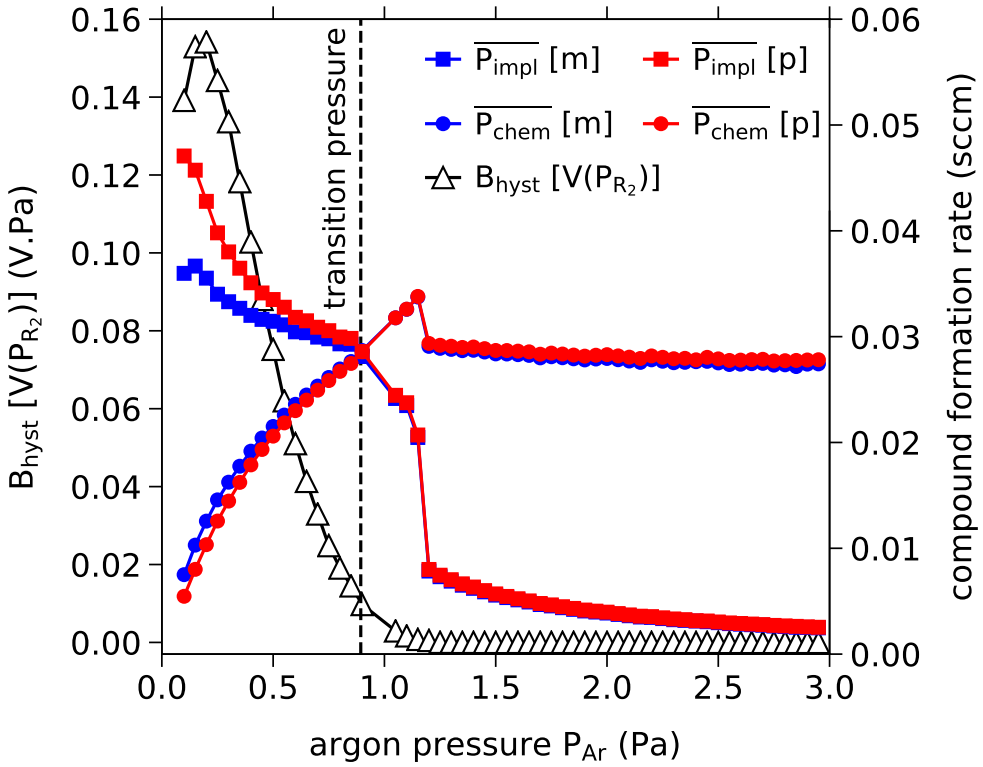

Figure 7: Influence of the argon pressure P_{Ar} on double hysteresis behavior. The reference from Appendix A is used, but with $\alpha_{\mathrm{t}} = 0.3$ and a varying argon pressure (bottom axis). Left axis: the double hysteresis area in the $V(P_{\mathrm{R}_2})$ process curve ($B_{\mathrm{hyst}}[V(P_{\mathrm{R}_2})]$, black). Right axis: the compound formation rates due to direct implantation P_{impl} and chemisorption P_{chem}, averaged over the metal (blue) or poison (red) branch. The double hysteresis area disappears in the regime for which $\overline{P_{\mathrm{chem}}} > \overline{P_{\mathrm{impl}}}$.

The vanishing behavior is similar to the influence of the target sticking coefficient (Figure 6). The reason for this similarity is the dependency difference of implantation and chemisorption on the argon pressure. Chemisorption de-

pends on the reactive gas partial pressure (Equation (4)), and therefore the argon pressure does not affect this process. In contrast, reactive ion implantation is proportional to the reactive gas fraction $f_{\mathrm{R}_2} = P_{\mathrm{R}_2}/(P_{\mathrm{R}_2} + P_{\mathrm{Ar}})$ which becomes smaller at a higher argon pressure. As such, when increasing the argon pressure, the compound formation rate by direct implantation decreases while the formation rate by chemisorption becomes more prominent.

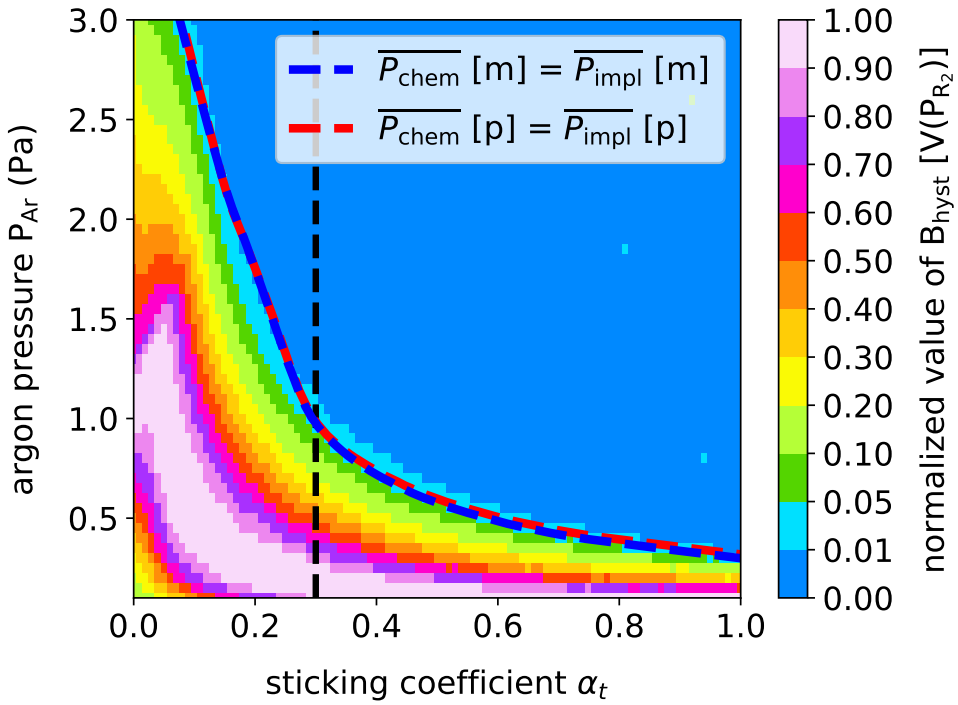

Figure 8: The double hysteresis area $B_{\mathrm{hyst}}[V(P_{\mathrm{R}_2})]$ as a function of the argon pressure and target sticking coefficient. The $B_{\mathrm{hyst}}[V(P_{\mathrm{R}_2})]$ values were normalized per sticking coefficient. The two solid lines indicate the condition of equal compound formation rate by chemisorption $\overline{P_{\mathrm{chem}}}$ and direct ion implantation $\overline{P_{\mathrm{impl}}}$, calculated for the metal (blue) and poison (red) branch. The dashed line corresponds with the data of Figure 7.

The above discussed analysis was repeated for different argon pressure and target sticking coefficient combinations. The results of these calculations are summarized in Figure 8 which depicts the (normalized) double hysteresis area $B_{\mathrm{hyst}}[V(P_{\mathrm{R}_2})]$ as a function of both parameters. The value of $B_{\mathrm{hyst}}[V(P_{\mathrm{R}_2})]$ numerically never reaches zero. Hence, the values were normalized per sticking coefficient to permit a relative comparison between the

different pressures. On the same figure, the condition of equal formation rate by chemisorption and direct implantation are shown as calculated for the metal (blue) and poison (red) branch.

It can be observed that the double hysteresis indeed vanishes when the aforementioned condition is reached. Indeed, a good agreement between the lines and the 1% or 5% contour line is observed. Hence, an important conclusion from Figure 8 is that at high values of the target sticking coefficient, no double hysteresis is observed, except at very low argon pressures. This means that it is difficult to observe double hysteresis for a target material on which the reactive gas strongly chemisorbes. Since many publications on hysteresis consider target materials with a relatively high sticking coefficient, this might also explain the deficit of double hysteresis in literature.

A careful inspection of Figure 8 shows a small decrease of $B_{\mathrm{hyst}}[V(P_{\mathrm{R}_2})]$ for a combination of an extremely low argon pressure and a low sticking coefficient (bottom left corner of the figure). This decrease can be traced back to an oversaturation of the subsurface based on the branch averaged values. The oversaturation is the result of the combination of a very large implantation flux and a very low sputtering flux. The effect is more pronounced in the poison branch. As a result of this, the rate of non-reacted implanted ions that escape from the target increases in the poison branch and converges to the corresponding rate in the metal branch. Observing such trend experimentally might thus be an indication of a very large concentration of non-reacted ions inside the target. Caution should however be taken with the interpretation of the results regarding the validity of the current RSD-model in this limit.

4. Discussion

The results in Section 3 can be understood in terms of the subsurface mechanism for double hysteresis proposed earlier [14]. This mechanism relates the magnitude of the double hysteresis to the rate of non-reacted implanted ions that are sputtered from the target in the transition from a metallic target to a poisoned target but not in the reverse transition. Based on the observations, chemisorption related parameters can be subdivided in two categories.

A first set of parameters is related to the chamber and substrate conditions. Though the hysteresis curve and the single hysteresis area are changed in a drastic way, the magnitude of the double hysteresis remains a conserved

quantity. This can be understood as follows. The conditions of the vacuum chamber and substrate determine to a large extend the balance between the reactive gas flow towards the substrate and the pump. When the substrate flow dominates, a large amount of reactive gas can be consumed by sputter deposition and the target remains metallic. This mechanism postpones the first critical point to larger reactive gas flows and induces the magnitude of the single hysteresis to increase. The sputter consumption does however not influence the state of the target subsurface and hence the double hysteresis behavior remains unaffected.

This is different when the affinity of the target material for chemisorption is considered. In this case, an increase of chemisorption affects the balance between the compound formation by chemisorption and direct implantation at the target. For either a sufficiently high sticking coefficient α_{t} or a sufficiently low implantation flux (high P_{Ar}), the poisoning of the target becomes disconnected from the subsurface mechanism that is driving the double hysteresis phenomenon. Indeed, when chemisorption dominates the surface target condition, the time for the implanted ions to react becomes independent of the compound fraction formed by ion implantation. Hence, the positive feedback loop that results in target poisoning by ion implantation [4] is no longer possible. This particular property of the reactive sputter process can be used to alter the double hysteresis behavior. For target materials such as Al where the sticking coefficient for oxygen is low, double hysteresis can be avoided by sputtering at sufficiently high argon pressures. On the other hand, it is possible to study double hysteresis for materials with a high sticking coefficient for oxygen such as Ti by measuring at sufficiently low argon pressures. An estimate of the argon pressure that is required for this can be made using Figure 8. Remark however that this plot has been obtained based on an Al reference system. Figure 8 could also be interpreted in a different way: when the sticking coefficient of the reactive gas is increased, the double hysteresis vanishes. This is achieved when e.g. the gas in front of the target surface is more ionized or dissociated, which may happen at elevated discharge current densities. The latter might play an important role in HiPIMS [18, 19].

Finally, some chamber conditions might influence both the balance between the reactive gas flows inside the vacuum chamber as well as the balance between compound formation by chemisorption and direct implantation. An example of this is the chamber temperature. When elevating the chamber temperature, the flow to the pump is decreased (Equation 2). This can be

linked via the critical points to an increase of the single hysteresis in a similar fashion as originally modeled by Berg and Nyberg [3]. On the other hand, target chemisorption is decreased (Equation (3)). The latter results in a target compound formation that is more dominated by direct implantation and an increase in double hysteresis. An important remark should be made regarding the target temperature. This temperature is not taken into account in the current model. According to the discussion in our previous work [14], effects of diffusion might play an important role in the subsurface mechanism, which are expected to decrease the double hysteresis for elevated temperatures. An experimental verification of this hypothesis would be of great interest for a better understanding of the subsurface mechanism.

5. Conclusion

A high-throughput analysis using a state-of-the-art code to predict process curves during reactive sputtering was used to study the influence of chemisorption on the double hysteresis behavior. Although the proposed subsurface mechanism that induces the double hysteresis is implantation driven, chemisorption significantly changes it under certain circumstances. The simulations explain how double hysteresis can be altered using the interplay between chemisorption and implantation. For example, the argon pressure can be adapted in order to avoid double hysteresis for materials with a low sticking coefficient such as Al. Or on the contrary: to induce and study double hysteresis for materials with a high sticking coefficient such as Ti. This opens a simple and direct experimental way to study the exact nature of double hysteresis.

Acknowledgments

The authors wish to acknowledge Ghent University for the financial support through the project TIMERS (grant number 01J05319). The main author would like to thank his family and loved ones for always supporting him.

Appendix A. Reference system

The same reference system as in Van Bever *et al.* [14] was used. This reference was obtained from fig. 14 and appendix B of Strijckmans *et al.*, [4]

where experimental data for an Al/O_2-system had been fitted. A minor correction was applied for the racetrack and experimental data for the secondary electron yield [20] were included. The data was refitted using the compound sputter yield and the effective substrate surface area. The fit successfully reproduces the experimental data for different pumping speeds [4]. The newly fitted compound sputter yield remains in good agreement with experimental data from Schelfhout *et al.* [21, 22]. The parameters are enlisted in Table I of Van Bever et al.[14].

References

[1] S. Berg, T. Nyberg, Fundamental understanding and modeling of reactive sputtering processes, Thin Solid Films 476 (2) (2005) 215–230. doi:10.1016/j.tsf.2004.10.051.

[2] K. Strijckmans, D. Depla, A time-dependent model for reactive sputter deposition, Journal of Physics D: Applied Physics 47 (23) (2014) 235302. doi:10.1088/0022-3727/47/23/235302.

[3] S. Berg, E. Särhammar, T. Nyberg, Upgrading the "Berg-model" for reactive sputtering processes, Thin Solid Films 565 (2014) 186–192. doi:10.1016/j.tsf.2014.02.063.

[4] K. Strijckmans, R. Schelfhout, D. Depla, Tutorial: hysteresis during the reactive magnetron sputtering process, Journal of Applied Physics 124 (24) (2018) 241101. doi:10.1063/1.5042084.

[5] E. Särhammar, K. Strijckmans, T. Nyberg, S. Van Steenberge, S. Berg, D. Depla, A study of the process pressure influence in reactive sputtering aiming at hysteresis elimination, Surface and Coatings Technology 232 (2013) 357–361. doi:10.1016/j.surfcoat.2013.05.035.

[6] D. Rosén, I. Katardjiev, S. Berg, W. Möller, TRIDYN simulation of target poisoning in reactive sputtering, Nuclear Instruments and Methods in Physics Research Section B: Beam Interactions with Materials and Atoms 228 (1) (2005) 193–197. doi:10.1016/j.nimb.2004.10.044.

[7] X. Y. Li, D. Depla, W. P. Leroy, J. Haemers, R. D. Gryse, Influence of deposition on the reactive sputter behaviour during rotating cylindrical magnetron sputtering, Journal of Physics D: Applied Physics 41 (3) (2008) 035203. doi:10.1088/0022-3727/41/3/035203.

[8] D. Depla, X. Y. Li, S. Mahieu, K. Van Aeken, W. P. Leroy, J. Haemers, R. De Gryse, A. Bogaerts, Rotating cylindrical magnetron sputtering: Simulation of the reactive process, Journal of Applied Physics 107 (11) (2010) 113307. doi:10.1063/1.3415550.

[9] F. G. Cougnon, K. Strijckmans, R. Schelfhout, D. Depla, Hysteresis behavior during facing target magnetron sputtering, Surface and Coatings Technology 294 (2016) 215–219. doi:10.1016/j.surfcoat.2016.03.096.

[10] W. D. Sproul, M. E. Graham, M.-S. Wong, P. J. Rudnik, Reactive d.c. magnetron sputtering of the oxides of Ti, Zr, and Hf, Surface and Coatings Technology 89 (1) (1997) 10–15. doi:10.1016/S0257-8972(96)02913-1.

[11] W. D. Sproul, D. J. Christie, D. C. Carter, Control of reactive sputtering processes, Thin Solid Films 491 (1) (2005) 1–17. doi:10.1016/j.tsf.2005.05.022.

[12] M. Aiempanakit, T. Kubart, P. Larsson, K. Sarakinos, J. Jensen, U. Helmersson, Hysteresis and process stability in reactive high power impulse magnetron sputtering of metal oxides, Thin Solid Films 519 (22) (2011) 7779–7784. doi:10.1016/j.tsf.2011.06.021.

[13] R. Schelfhout, K. Strijckmans, D. Depla, The existence of a double S-shaped process curve during reactive magnetron sputtering, Applied Physics Letters 109 (11) (2016) 111605. doi:10.1063/1.4962958.

[14] J. Van Bever, K. Strijckmans, D. Depla, A computational study of the double hysteresis phenomenon during reactive sputtering, Journal of Physics D: Applied Physics 55 (35) (2022) 355302. doi:10.1088/1361-6463/ac761c.

[15] K. Strijckmans, Modeling the reactive magnetron sputtering process, dissertation, Ghent University (2015).

[16] The RSD software can be freely downloaded from www.draft.ugent.be (2021).

[17] The RSDplot software is available on request (2021).

[18] F. Moens, S. Konstantinidis, D. Depla, The target material influence on the current pulse during high power pulsed magnetron sputtering, Frontiers in Physics 5 (2017) 00051. doi:10.3389/fphy.2017.00051.

[19] K. Strijckmans, F. Moens, D. Depla, Perspective: Is there a hysteresis during reactive high power impulse magnetron sputtering (r-HiPIMS)?, Journal of Applied Physics 121 (8) (2017) 080901. doi:10.1063/1.4976717.

[20] D. Depla, S. Mahieu, R. De Gryse, Magnetron sputter deposition: linking discharge voltage with target properties, Thin Solid Films 517 (9) (2009) 2825–2839. doi:10.1016/j.tsf.2008.11.108.

[21] R. Schelfhout, K. Strijckmans, D. Depla, Sputter yield measurements to evaluate the target state during reactive magnetron sputtering, Surface and Coatings Technology 399 (2020) 126097. doi:10.1016/j.surfcoat.2020.126097.

[22] R. Schelfhout, K. Strijckmans, D. Depla, Anomalous effects in the aluminum oxide sputtering yield, Journal of Physics D: Applied Physics 51 (15) (2018) 155202. doi:10.1088/1361-6463/aab321.